OPEN

Different Impact of Gadopentetate and Gadobutrol on Inflammation-Promoted Retention and Toxicity of Gadolinium Within the Mouse Brain

Lina Anderhalten, MD,* Rafaela V. Silva, MSc,*† Anna Morr, MSc,‡ Shuangqing Wang, MD,*
Alina Smorodchenko, MD,§ Jessica Saatz, PhD,‖ Heike Traub, PhD,‖ Susanne Mueller, MSc,¶**
Philipp Boehm-Sturm, PhD,¶** Yasmina Rodriguez-Sillke, PhD,†† Désirée Kunkel, PhD,††
Julia Hahndorf, MSc,‡ Friedemann Paul, MD,* Matthias Taupitz, MD,‡
Ingolf Sack, PhD,‡ and Carmen Infante-Duarte, PhD*

Objectives: Using a murine model of multiple sclerosis, we previously showed that repeated administration of gadopentetate dimeglumine led to retention of gadolinium (Gd) within cerebellar structures and that this process was enhanced with inflammation. This study aimed to compare the kinetics and retention profiles of Gd in inflamed and healthy brains after application of the macrocyclic Gd-based contrast agent (GBCA) gadobutrol or the linear GBCA gadopentetate. Moreover, potential Gd-induced neurotoxicity was investigated in living hippocampal slices ex vivo.

Materials and Methods: Mice at peak of experimental autoimmune encephalomyelitis (EAE; n = 29) and healthy control mice (HC; n = 24) were exposed to a cumulative dose of 20 mmol/kg bodyweight of either gadopentetate dimeglumine or gadobutrol (8 injections of 2.5 mmol/kg over 10 days). Magnetic resonance imaging (7 T) was performed at baseline as well as at day 1, 10, and 40 post final injection (pfi) of GBCAs. Mice were sacrificed after magnetic resonance imaging and brain and blood Gd content was assessed by laser ablation-inductively coupled plasma (ICP)-mass spectrometry (MS) and ICP-MS, respectively. In addition, using chronic organotypic hippocampal slice cultures, Gd-induced neurotoxicity was addressed in living brain tissue ex vivo, both under control or inflammatory (tumor necrosis factor α [TNF-α] at 50 ng/μL) conditions.

Results: Neuroinflammation promoted a significant decrease in T1 relaxation times after multiple injections of both GBCAs as shown by quantitative T1 mapping of EAE brains compared with HC. This corresponded to higher Gd retention within the EAE brains at 1, 10, and 40 days pfi as determined by laser ablation-ICP-MS. In inflamed cerebellum, in particular in the deep cerebellar nuclei (CN), elevated Gd retention was observed until day 40 after last gadopentetate application (CN: EAE vs HC, 55.06 ± 0.16 μM vs 30.44 ± 4.43 μM). In contrast, gadobutrol application led to a rather diffuse Gd content in the inflamed brains, which strongly diminished until day 40 (CN: EAE vs HC, 0.38 ± 0.08 μM vs 0.17 ± 0.03 μM). The analysis of cytotoxic effects of both GBCAs using living brain tissue revealed an elevated cell death rate after incubation with gadopentetate but not gadobutrol at 50 mM. The cytotoxic effect due to gadopentetate increased in the presence of the inflammatory mediator TNF-α (with vs without TNF-α, 3.15% ± 1.18% vs 2.17% ± 1.14%; P = 0.0345).

Conclusions: In the EAE model, neuroinflammation promoted increased Gd retention in the brain for both GBCAs. Whereas in the inflamed brains, efficient clearance of macrocyclic gadobutrol during the investigated time period was observed, the Gd retention after application of linear gadopentetate persisted over the entire observational period. Gadopentetate but not gadubutrol appeared to be neurotoxic in an ex vivo paradigm of neuronal inflammation.

Gadolinium-based contrast agents (GBCAs) are commonly used in contrast-enhanced magnetic resonance imaging (MRI) because of their ability to improve the visibility of internal body structures by increasing the relaxation rate of nearby water protons in vivo.[1] The diagnostic application of GBCAs is currently considered largely safe in patients with normal renal function. However, after repeated administration of mainly linear GBCAs, retention of gadolinium (Gd) within different organs was reported to occur in patients without renal impairment.[2,3] This resulted in restrictions on the use of linear GBCAs by the European Medicines Agency (EMA/625317/2017)[4] and class warnings by the US Food and Drug Administration.[5]

Within central nervous system (CNS) structures, Kanda et al[6] revealed for the first time a positive correlation between previous administrations of linear GBCAs and T1 hyperintensities in unenhanced brain MRI scans, in particular in the dentate nucleus (DN). These observations were confirmed by several other authors in humans[7–12] and rodent models,[13–19] principally after repeated application of linear GBCAs. Moreover, Gd retention in neuronal parenchyma, especially inside the DN, was quantitatively assessed by inductively coupled plasma mass spectrometry (ICP-MS) or laser ablation ICP-MS (LA-ICP-MS)[17,20–26] after in vivo GBCA administration.

The risk of interstitial retention is especially high for the kinetically less stable linear GBCAs compared with macrocyclic agents.[27,28] It is suggested that linear GBCAs partially dechelate in vivo, leading to transmetallation with endogenous cations such as calcium,[29] iron,[30] or zinc,[31] resulting in long-term retention inside the brain. Contrary to that, macrocyclic GBCAs are expected to be washed out continuously in the form of the intact chelate,[17,32] following specific clearance kinetics for the different macrocyclic compounds.[33,34]

In the context of chronic inflammation of the CNS such as in multiple sclerosis, GBCAs are primarily applied to determine the magnitude of blood-brain barrier (BBB) disruption and to estimate the number of active inflammatory lesions within the CNS.[35] Hence, the concern for Gd retention is particularly relevant for patients with multiple sclerosis because GBCA-MRI is commonly used for initial diagnosis as well as for monitoring both clinical course and treatment response.[36] Moreover, we previously reported using the experimental autoimmune encephalomyelitis (EAE) model that neuroinflammation may facilitate the retention of Gd in the mouse brains. We showed that 10 days after repeated gadopentetate injections, Gd levels were higher within inflamed brains compared with healthy controls (HCs) and demonstrated the formation of an elevated number of submicrometric Gd hotspots in the deep cerebellar nuclei (CN) of EAE mice.[37]

However, it has not yet been clarified for how long Gd may be retained in the inflamed CNS compared with healthy CNS, what factors may contribute to brain retention, how linear and macrocyclic GBCAs differ in terms of magnitude and kinetics of retention, and how Gd may affect neuronal tissue under inflammatory conditions. Therefore, we aimed to monitor and quantify Gd retention in brain tissue by MRI and LA-ICP-MS after repeated administration of either the linear gadopentetate or the macrocyclic gadobutrol in both healthy and EAE mice in vivo. Furthermore, using the well-established ex vivo model of organotypic hippocampal slice culture, we assessed Gd toxicity and how an inflammatory milieu may affect its toxic potential.

MATERIALS AND METHODS

Mouse Model of EAE and Study Design

Animal experiments were conducted in accordance with national and institutional guidelines for the care and use of laboratory animals and with directive 2010/63/EU of the European Parliament and of the Council of 22 September 2010 and were approved by the Berlin State Office for Health and Social Affairs (LAGeSo, registration number G106/19). Experimental autoimmune encephalomyelitis was actively induced in 9- to 12-week-old SJL/J female mice (Janvier Labs, France; n = 29) by subcutaneous immunization with 250 μg proteolipid protein peptide (PLP$_{139-151}$; purity 95%; Pepceuticals, Leicester, United Kingdom) and 800 μg *Mycobacterium tuberculosis* H37Ra (Difco, Franklin Lakes, NJ) diluted in 100 μL complete Freund's adjuvant. In addition, 250 ng pertussis toxin (List, Biological Laboratories, Campbell, CA) were injected intraperitoneally on day 0 (day of immunization) and day 2 of the study. The EAE mice were monitored daily for clinical deficiency as follows: 0 = no disease; 1 = complete tail paralysis; 2 = hindlimb paresis; 3 = hindlimb plegia; 4 = paraplegia and forelimb weakness; and 5 = moribund or death. Experimental autoimmune encephalomyelitis (n = 29) and HC (n = 24) mice were exposed to 8 intravenous injections via the tail vein of either a linear GBCA (gadopentetate dimeglumine; Magnevist, Bayer, Germany, n = 27) or a macrocyclic GBCA (gadobutrol; Gadovist, Bayer, n = 26) at 2.5 mmol/kg body weight (BW), which corresponds to a cumulative dose of 20 mmol/kg BW. As displayed in Figure 1A, 4 consecutive daily injections of either gadopentetate or gadobutrol were followed by a 2-day break to reduce stress for the animals and 4 additional injection days as described previously.[37] The GBCA applications started on day 12 to 13 postimmunization when EAE mice showed a peak of disability. The EAE mice presented first clinical signs on days 8 to 10, reached maximal clinical disability on day 12 to 13, and further showed a relapsing-remitting course until day 64 (Fig. 1B). No significant differences in EAE score between the time points of

LA-ICP-MS, comparing the gadopentetate and gadobutrol groups, were detected (Kruskal-Wallis test; all EAE animals killed at respective time points [n = 4–5], P = 0.7509; EAE animals examined using LA-ICP-MS [n = 2], P = 0.3824).

MRI and Image Data Analysis

Whole-brain coronal MRI scans were performed in vivo in EAE and HC mice on a 7 T small-animal scanner (Bruker PharmaScan, Ettlingen, Germany), running ParaVision 6.1 software at baseline (immediately before the first GBCA injection) and 1, 10, and 40 days post final injection (pfi) of either a linear or a macrocyclic GBCA. Measurements were conducted using a 72-mm linear volume coil for excitation (RAPID Biomedical GmbH, Rimpar, Germany) and a mouse head surface coil (Bruker, Ettlingen, Germany). T1 map image acquisition was conducted using an axial 2-dimensional rapid acquisition with relaxation enhancement at variable repetition times (RARE-VTR) sequence (echo time, 9.83 milliseconds; 8 repetition times from 255 to 7000 milliseconds; rare factor = 2; field of view, 19.2 mm^2; matrix, 128 × 128; number of slices = 10; slice thickness, 1 mm; scan time, 17 minutes 13 seconds). During imaging, mice were anesthetized with 1.0% to 1.5% isoflurane in 30% O_2 and 70% N_2O administered via face mask, and gently fixed to the head coil to reduce motion and breathing artifacts. To maintain body temperature constant, animals were placed on a bed with circulating heated water. Respiration was monitored using a pressure-sensitive pad placed on the thorax (Small Animal Instruments Inc, Stony Brook, NY).

Magnetic resonance imaging data were registered to the Allen mouse brain atlas (ABA), as described elsewhere,[38] in a blinded manner using an in-house developed MATLAB toolbox ANTx (available under https://github.com/ChariteExpMri/antx2). The T1 relaxation times of each single ABA brain structure were calculated using the back-transformed atlas, which matched the individual magnetic resonance images. The quantitative relaxometry assessment of Gd retention does not require any reference region. Differences in T1 relaxation time between baseline MRI and MRI at the different time points pfi of GBCAs were quantified as T1 relaxation time change (T1 change (%) = (T1$_{pfi of GBCA}$ − T1$_{baseline}$)/T1$_{baseline}$ * 100). In animals with enlarged ventricles due to neuroinflammation, atlas transformation was corrected by subtracting the individual ventricle masks segmented on T2-weighted images using Analyze 10.0 (AnalyzeDirect, Inc).

Tissue Processing and Histology

Mice were sacrificed with an overdose of ketamine/xylazine either 1, 10, or 40 days pfi of GBCAs (n = 4–5 mice/time point). Blood was collected and animals were immediately transcardially perfused with 0.1 M PBS at a continuous perfusion speed of 40 rpm (U/min; Ismatec ISM444B-115 V Analog Peristaltic Pump). Brains were extracted, fixed in 4% paraformaldehyde (PFA) and 30% sucrose, embedded and frozen (−80°C) for subsequent histological examinations. For histology, brains were cut coronally separating the forebrain, midbrain, and cerebellum. Frozen brain sections were cut in the coronal plane into 10-μm-thick cryosections and stored at −80°C. Consecutive frozen sections of those chosen for LA-ICP-MS were stained with hematoxylin and eosin (H&E) according to the standard protocol to assess inflammation. Hematoxylin and eosin images were acquired at ×2 and ×10 magnifications with a Keyence Fluorescence Microscope (BZ-X800, Germany) using the bright field mode.

LA-ICP-MS of Cerebellar Slices

The LA-ICP-MS analysis of 10-μm-thick cerebellar cryosections was performed on a commercial LA system (NWR-213; ESI, Bozeman, MT) equipped with a 2-volume sample chamber coupled to a sector field ICP-MS (Element XR; Thermo Fisher Scientific, Bremen, Germany). A Y-piece was used to add argon to the helium carrier gas before entering the plasma. The ICP-MS was tuned daily for maximum ion intensity, signal stability (relative standard deviation <5%), and oxide ratio (ThO/Th <1%) during continuous ablation on a microscopic glass slide.
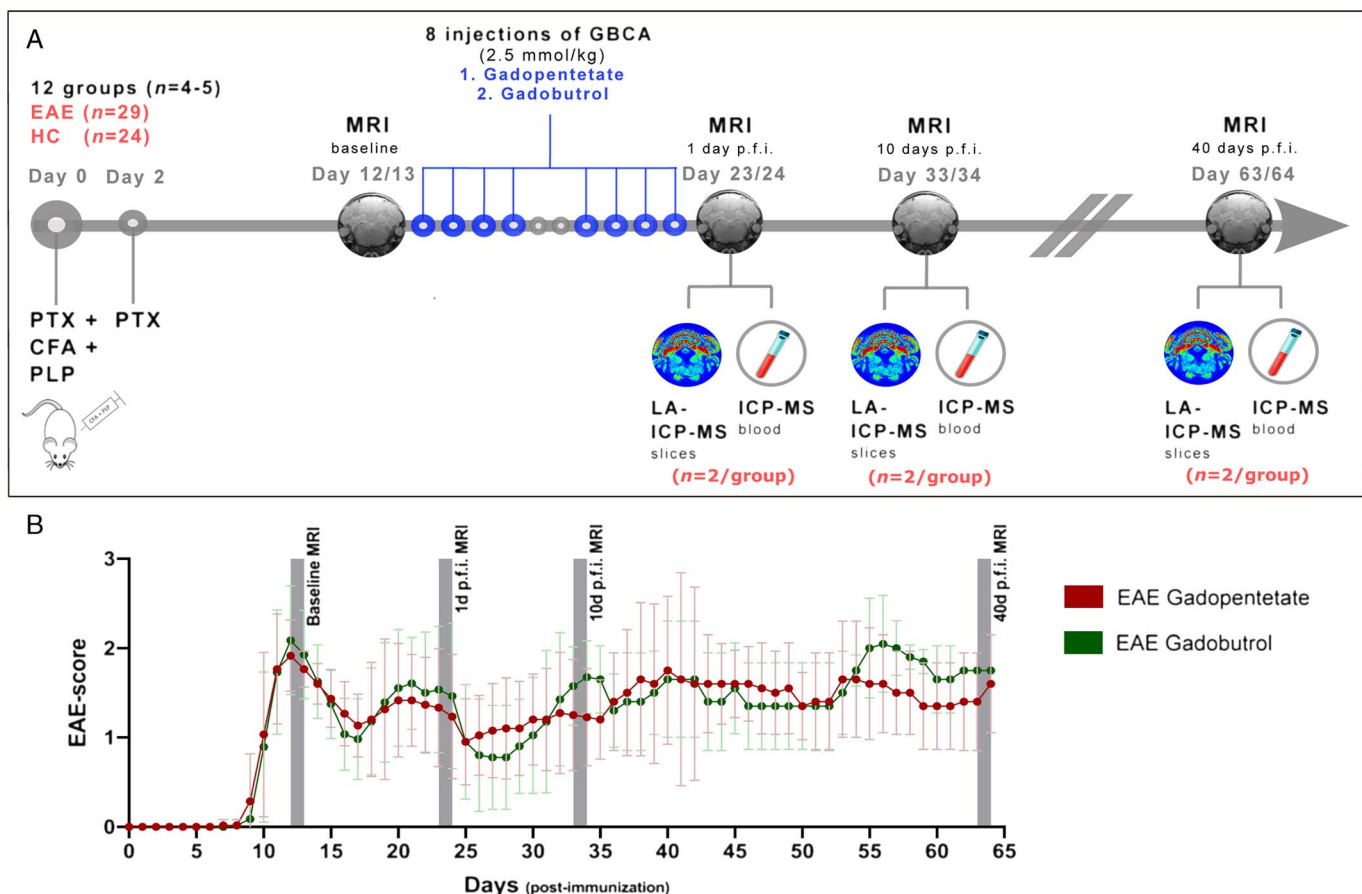
FIGURE 1. Animal study design. A, Schematic illustration of the in vivo setup. A total of 24 HC and 29 EAE mice received 8 intravenous injections of either gadopentetate or gadobutrol at 2.5 mmol/kg BW (cumulative dose: 20 mmol/kg BW, 2-day pause after 4 consecutive applications). Mice underwent a baseline MRI before the first injection and further scans at day 1, 10, and 40 pfi of GBCAs. In EAE mice, baseline MRI started on day 12 to 13 postimmunization (peak of disease). After the MRI scans, 4 to 5 animals per group were sacrificed; brains were processed for LA-ICP-MS, and blood was collected for ICP-MS (n = 2/group). B, Clinical course of EAE animals based on the EAE score (mean ± SD). Red: gadopentetate-treated animals (n = 15), green: gadobutrol-treated animals (n = 14).

Instrumental parameters of the ICP-MS system include radio frequency (RF) power: 1350 W; plasma gas flow (Ar): 16 L min^{-1}; sample gas flow (Ar): 0.660 L min^{-1}; auxiliary gas flow (Ar); 1.05 L min^{-1}; mass resolution: 300 m/Δm; scanning mode: line by line; detected isotopes: ^{31}P, ^{34}S, ^{44}Ca, ^{55}Mn, ^{57}Fe, ^{65}Cu, ^{66}Zn, ^{153}Eu, ^{158}Gd, and ^{160}Gd. Parameters of the LA system include wavelength: 213 nm; helium gas flow: 1 L min^{-1}; laser fluence: 1.9 J cm^{-2}; spot size: 100 μm; scan speed: 100 μm s^{-1}; repetition rate: 20 Hz; and line overlap: 20 μm. Data visualization was done in Origin 2018 (OriginLab Corporation, Northampton, MA). Calibration for ^{65}Cu, ^{66}Zn, and ^{158}Gd (translation of count per spot of ablation [CPS] into fg/pixel) and drift correction was carried out by measuring matrix-matched standards cast on glass slides using analyte spiked agarose gels (analyte contents 0–310 fg/pixel).[39] For further analysis of Gd retention in the whole cerebellar slice (mean), DN, and CN, manual regions of interest (ROIs) were applied to the calibrated LA-ICP-MS images of ^{158}Gd. The analysis of each region was conducted 3 times in an independent randomized manner using ImageJ software[40] for better reliability, and obtained Gd concentrations were averaged. Calibrated concentrations of ^{66}Zn and ^{158}Gd (fg/pixel) were translated into molar values (μM) where 1 pixel corresponded to 80 μm × 22 μm × 10 μm (1.76 × 10^{-11} L) of brain volume.

Analysis of Blood Samples by ICP-MS

Blood samples were thawed and digested by a high-pressure asher (HPA-S, Anton Paar GmbH, Graz, Austria). In brief, 0.5 mL subboiled nitric acid (HNO$_3$, 65%) was added to 100 mg of each blood sample and incubated overnight. Thereafter, samples were incinerated for 3 hours at 300°C. After cooling, the digested samples were diluted to a volume of 5 mL with MilliQ water. Samples were measured with an Element 2 ICP sector field mass spectrometer (Thermo Fisher Scientific) in combination with the autosampler 4DXF-73A (ESI Elemental Service & Instruments GmbH, Mainz, Germany). Calibration was carried out by standard addition of diluted multielement ICP standards. Blood control samples were obtained from an unmanipulated age- and sex-matched mouse. Instrumental parameters of the ICP-MS system for blood analysis include RF power: 1250 W; plasma gas flow (Ar): 16 L min^{-1}; sample gas flow (Ar): 1.215 L min^{-1}; auxiliary gas flow (Ar); 1.05 L min^{-1}; mass resolution: 4000 m/Δm; detected isotopes: ^{55}Mn, ^{115}In, ^{155}Gd, ^{156}Gd, ^{157}Gd, ^{158}Gd, and ^{160}Gd.

Generation of Chronic Organotypic Hippocampal Slices and Applied Culture Conditions

SJL/J pups (7–10 days) were decapitated, brains removed, and hippocampi extracted and sectioned coronally into 350-μm-thick slices using a McIlwain Tissue Chopper (Mickle Laboratory Engineering Co Ltd, UK). Six single slices from different mice were placed on 1 membrane of a cell culture insert (Millicell inserts, Merck, Germany) in a 6-well plate with 2 mL prewarmed (37°C) and oxygenized modified Opitz-Araya slice culture medium (SCM; 75% minimum essential

medium (MEM) ×1, 20% normal horse serum heat-inactivated, 30 mM N-2-hydroxyethylpiperazine-N-2-ethane sulfonic acid (HEPES), 13 mM D-glucose, 5.2 mM NaHCO₃, 2 mM MgSO₄, 1 mM L-glutamine, 1 mM CaCl₂, 1 mg/L insulin-transferrin-selenium supplement, 0.004% ascorbic acid, pen/strep) per well.[41] Chronic slices were cultured for 12 days at 37°C and 5% CO₂; SCM was changed every 2 days. From day 13 on, treatment with tumor necrosis factor α (TNF-α; mouse recombinant, lyophilized; Invitrogen) and the 2 different GBCAs (gadopentetate and gadobutrol) was initiated as displayed in Figure 2. To mimic inflammation, TNF-α at 50 ng/mL was added to half of the slices for a 48-hour preincubation period. On day 15, medium was exchanged and either gadopentetate or gadobutrol diluted in SCM was added on the top of the membranes at 1, 10, or 50 mM, respectively. In control cultures, no GBCA was applied. In addition, TNF-α at 50 ng/mL was added again to the corresponding slices for simultaneous coincubation with the GBCAs for an additional 48 hours. In positive control slices only, N-methyl-D-aspartic acid (NMDA) at 50 μM was added on day 16 for 4 hours to induce neurotoxicity.

Tissue Processing and Histology of the Chronic Hippocampal Slices

Treatment of slices with GBCAs ± TNF-α was stopped on day 17 by washing the membranes with fresh SCM. To assess cell death, propidium iodide (PI) was added to each well at 10 μg/mL for 30 minutes at 37°C. Further steps were performed without direct illumination to prevent photobleaching of the PI fluorophore. Subsequently, the membrane inserts were washed twice in prewarmed SCM for 10 minutes, followed by 1-hour fixation in 4% PFA. Thereafter, the membranes were transferred into sucrose (30%) in 0.1 M PBS for 2 days for further fixation. After fixation, slices were removed from the membranes and processed for cryosectioning. Cryostat slicing was performed at a thickness of 20 μm for assessment of the cell death ratio, at 10 μm for imaging mass cytometry (IMC) measurements. To analyze the cell death rate, hippocampal cryosections were counterstained with 4′,6-diamidin-2-phenylindol (DAPI) and subsequently mounted in a mounting medium (Thermo Fisher Scientific, Shandon Immu-Mount). Negative and positive controls were pooled for further analysis using fluorescence microscopy. Three independent rounds of experiments were conducted according to the experimental setup shown in Figure 2.

Fluorescence Microscopy and Toxicity Assay

Fluorescence images were taken from the section of the middle layer of slices and acquired using a Keyence Fluorescence Microscope (BZ-X800, Germany). Overview snapshots at ×2 magnification (CFI Plan Apo Lambda 2x; numerical aperture: 0.10, working distance: 8.50 mm) were taken in the DAPI filter line (BZ-X filter DAPI, model OP-87762; excitation wavelength: 360/40 nm, emission wavelength: 460/50 nm) for orientation. Thereupon, the dentate gyrus (DG) was imaged at ×20 magnification (CFI Plan Apo Lambda 20x; numerical aperture: 0.75, working distance: 1.00 mm). Only those DGs that passed the following criteria were imaged: (1) DG and hippocampal C1 region were distinguishable; (2) the original DG shape was maintained; and (3) neuronal cells of DG were in a good focus and distinguishable. Resulting DGs were imaged for DAPI fluorescence in the DAPI filter line and PI fluorescence in the Texas Red filter line (BZ-X filter TexasRed, model OP-87765; excitation wavelength: 560/40 nm, emission wavelength: 630/75 nm). Photobleaching was minimized by reducing laser power and exposure time between image acquisitions. Per treatment group 8 to 12 DG images were obtained. All images were blindly analyzed using ImageJ software.[40] In stacks combining PI fluorescence and DAPI fluorescence images, manual ROIs around the single DG were drawn and the cell death rate was calculated (%, proportion of PI+ cells to DAPI+ cells). Recounting by independent investigators revealed a mean count-recount difference of 0.18% in cell death rate and a maximal count-recount difference of 1%.

Imaging Mass Cytometry

Gadolinium-based contrast agent penetration within the chronic slices during the 48 hours of incubation was quantified by IMC of 10-μm-thick cryosections. Two untreated control sections, 2 sections treated with 10 mM gadopentetate, and 2 treated with 10 mM gadobutrol were ablated. Before the ablation process, nucleic acids were labeled with Iridium-Cell-IDTM Intercalator (125 μM; Fluidigm, Canada) according to IMC staining protocols (available at www.fluidigm.com) for subsequent colocalization of nucleic acids with elemental Gd. Imaging mass cytometry was performed on a CyTOF2/upgraded to Helios
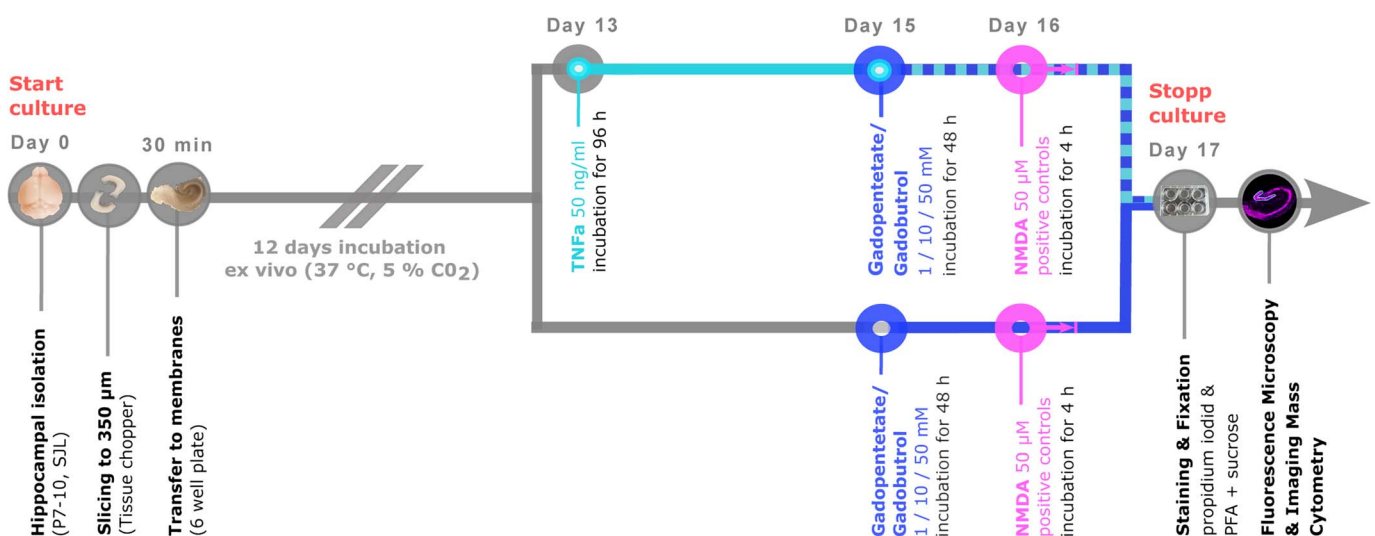
FIGURE 2. Schematic illustration of the ex vivo study design. Organotypic hippocampal slices were incubated for 12 days after initial preparation. On day 13 treatment with TNF-α at 50 ng/mL was started in half of the slices (total incubation time: 96 hours). On day 15, treatment with either gadopentetate or gadobutrol was initiated (total incubation time: 48 hours), whereas simultaneous incubation with TNF-α at 50 ng/mL was continued. Incubation with NMDA for 4 hours was performed in positive control slices only on day 16. On day 17, the chronic cultures were terminated, followed by live staining with PI and further fixation in PFA and sucrose. Cell viability was assessed using fluorescence microscopy; IMC was conducted to visualize Gd tissue content.

specifications coupled to a Hyperion Tissue Imager (Fluidigm, Canada), using CyTOF software version 7.0.8493. The instrument was tuned according to the manufacturer's instructions, using the 3-Element Full Coverage Tuning Slide (Fluidigm, Canada). The dried slide was loaded into the imaging module and ROIs were selected for each sample on a preview (panorama). Optimal laser power was determined for each sample to obtain complete ablation of the tissue. Laser ablation was performed at a resolution of 1 μm and a frequency of 200 Hz in a mass range of 75 to 209 Da. Data were stored as MCD files. For semiquantitative comparison of the elemental content of Gd inside the ablated hippocampal slices, the mean ion count of 6 ROIs per DG of defined size (100 μm × 100 μm) was calculated using the MCD Viewer v1.0.560.6. The mean ion counts of the 2 ablated hippocampal slices per treatment group were averaged.

Statistical Analysis

Data were analyzed using the GraphPad Prism software (version 8.4.3; GraphPad Software, San Diego, California). Normal distribution of the variables was assessed using 3 normality tests (Shapiro-Wilk normality test, D'Agostino and Pearson normality test, and Anderson-Darling test); all data shown here were considered nonparametric. Values were expressed as geometric means and standard deviations. Two-group comparisons were performed by Mann-Whitney tests applying the Bonferroni correction for multiple testing over 3 consecutive time points. Because of the low sample size (n = 2 per group), merely descriptive statistics are shown for ^{158}Gd and ^{66}Zn concentrations measured using LA-ICP-MS and ICP-MS. As this was contemplated as an exploratory pilot study, no formal hypothesis testing was initially planned. Comparisons between more than 2 groups were accomplished by the Kruskal-Wallis test for nonparametric data followed by Dunn's post hoc test for multiple rank comparisons (α power = 0.05). Correlations among T1 relaxation times and the amount of detected Gd in cerebellar tissue were computed by the nonparametric Spearman rank correlation. P values <0.05 were indicative of significant group differences. The significance level of shown data was further displayed as * implying $P < 0.05$, ** implying $P < 0.01$, *** implying $P < 0.001$, and **** implying $P < 0.0001$.

RESULTS

Inflammation Promotes Long-term Gd Retention After Gadopentetate but Not Gadobutrol Application

To assess the effects of neuroinflammation on Gd retention after multiple injections of either linear gadopentetate or macrocyclic gadobutrol, T1 map RARE-VTR magnetic resonance images were acquired at day 1, 10, and 40 pfi (Fig. 3A). T1 relaxation time change (%) was calculated for the different brain areas that have been reported to retain Gd, including cerebellum (C), DN, CN, globus pallidus, thalamus, pons, medulla, hippocampus, and DG (supplementary Figure SDC 1, http://links.lww.com/RLI/A703). Whereas in HC animals, gadopentetate but not gadobutrol applications led to a negative T1 time change in the studied brain areas until 40 days pfi, in the EAE brain areas, both GBCAs appeared to be retained with similar regional distribution, although less pronounced for gadobutrol. Significant differences in T1 time change between inflamed and healthy brains at 24 hours pfi were observed for both linear gadopentetate and macrocyclic gadobutrol. Areas affected included the whole cerebellum, C, DN, CN, globus pallidus, thalamus, pons, medulla, hippocampus, and DG (supplementary Figure SDC 1, http://links.lww.com/RLI/A703).

Especially the cerebellar ROIs (C, DN, and CN) were identified as regions showing differences in T1 relaxation time change (%) between EAE and HC animals, as displayed in Figure 3B. Strikingly, differences between cerebellar ROIs of EAE and HC animals remained significant until 40 days pfi of gadopentetate (C, −10.61% ± 2.87% vs −2.76% ± 3.03%, P = 0.0477; DN, −15.13% ± 4.72% vs −3.64% ± 5.94%, P = 0.0477; CN, −13.69% ± 4.53% vs

−2.64% ± 4.31%, P = 0.0477). Within the EAE group, T1 time change even increased when comparing 10 and 40 days pfi of gadopentetate, in particular within the DN and CN, suggesting long-term Gd retention within these areas. Contrary to that, as shown in Figure 3B, 10 and 40 days pfi of gadobutrol, no significant differences between EAE and HC ROIs regarding T1 changes were detected (C, −1.95% ± 3.30% vs 0.83% ± 1.67%; DN, 1.95% ± 4.03% vs 4.95% ± 7.75%; CN, −1.93% ± 3.96% vs −0.33% ± 2.89%), suggesting a continuous clearance of gadobutrol from the brain toward day 40 pfi also in the inflamed tissue.

LA-ICP-MS Confirmed Regional Patterns and Kinetics of Gd Retention in Inflamed Versus Healthy Brains

Gadolinium retention inside the brain, as well as the distribution of different elements including zinc (Zn), copper (Cu), calcium (Ca), phosphorus (P), sulfur (S), manganese (Mn), and iron (Fe), was confirmed and quantified by LA-ICP-MS in representative 10-μm-thick cerebellar cryosections (n = 2 per group). Consecutive H&E-stained sections were imaged for localization of cerebellar ROIs (Fig. 4A).

Confirming MRI data, differences in Gd content between EAE and HC animals were obvious for both administered GBCAs (Fig. 4B). Whereas HC tissues retained Gd strictly limited to the areas of CN (including DN), the EAE cerebella presented Gd additionally localized within the granular layers of the cerebellar cortex, reaching mean Gd concentrations of 41.24 ± 6.97 μM on day 40 pfi of gadopentetate (Fig. 4B). In contrast, administration of gadobutrol led to a qualitatively much lower and diffuse Gd retention around the fourth ventricle (periventricular) and within the choroid plexus, as well as among marginal parts of the cerebellar cortex (Fig. 4B). The highest Gd levels were detected in brains of EAE animals receiving gadopentetate at all given time points of ablation. Gadolinium levels were 2- to 3-fold higher in EAE animals compared with HC mice at all measured time points, that is, 24 hours and 10 and 40 days pfi of gadopentetate, in particular inside the whole cerebellar slice (2.05–3.65-fold), the DN (1.66–2.03-fold), and CN (1.81–2.12-fold) (Fig. 4C). Interestingly, there was a trend of increasing Gd levels at day 40 pfi of gadopentetate in both EAE and HC mouse brains (EAE vs. HC; C, 11.51 ± 0.64 μM vs 3.15 ± 0.24 μM; DN, 49.03 ± 4.73 μM vs 29.46 ± 0.57 μM; CN, 55.06 ± 0.16 μM vs 30.44 ± 4.43 μM).

Regarding gadobutrol, Gd levels inside the C, DN, and CN were approximately 2- to 3-fold higher in EAE animals than HC mice 24 hours pfi. These levels were reduced at day 10 within all assessed brain areas but still higher in EAE. On day 40 pfi, Gd levels diminished to less than 0.40 μM regarding both EAE and HC animals as shown in Figure 4C (EAE vs HC: C, 0.28 ± 0.03 μM vs 0.14 ± 0.04 μM; DN, 0.37 ± 0.08 μM vs 0.17 ± 0.04 μM; CN, 0.38 ± 0.08 μM vs 0.17 ± 0.03 μM).

In particular, in the inflamed CN, administrations of gadopentetate resulted in retention of Gd 24 hours pfi approximately 4-fold higher compared with gadobutrol (DN, 4.43-fold; CN, 4.13-fold) and 7 to 8-fold higher regarding HC (DN, 8.53-fold; CN, 7.14-fold) (Fig. 4C). Differences between both GBCAs became more apparent on day 40, as Gd amounts pfi of gadopentetate were even increased, in contrast to strongly reduced Gd concentrations found after gadobutrol administration (Fig. 4C).

In addition, as shown in the supplementary Figure SDC 2A, http://links.lww.com/RLI/A704, we demonstrated an inverse correlation of Gd concentrations and mean T1 relaxation times for all 3 analyzed cerebellar ROIs, that is C (r_s = −0.93, $P < 0.0001$), DN (r_s = −0.74, P = 0.0078), and CN (r_s = −0.78, P = 0.0043) (see Supplemental Digital Content, Figure SDC 2A, http://links.lww.com/RLI/A704).

Gd Was Detectable in Blood Samples 40 Days pfi of Both Tested GBCAs

To evaluate the potential mobilization of Gd from organs to the blood circulation during the observation period, Gd concentrations (μg/g blood) in blood samples of EAE mice (n = 2/time point) and HC mice (n = 2/time point) were assessed by ICP-MS. Elevated Gd
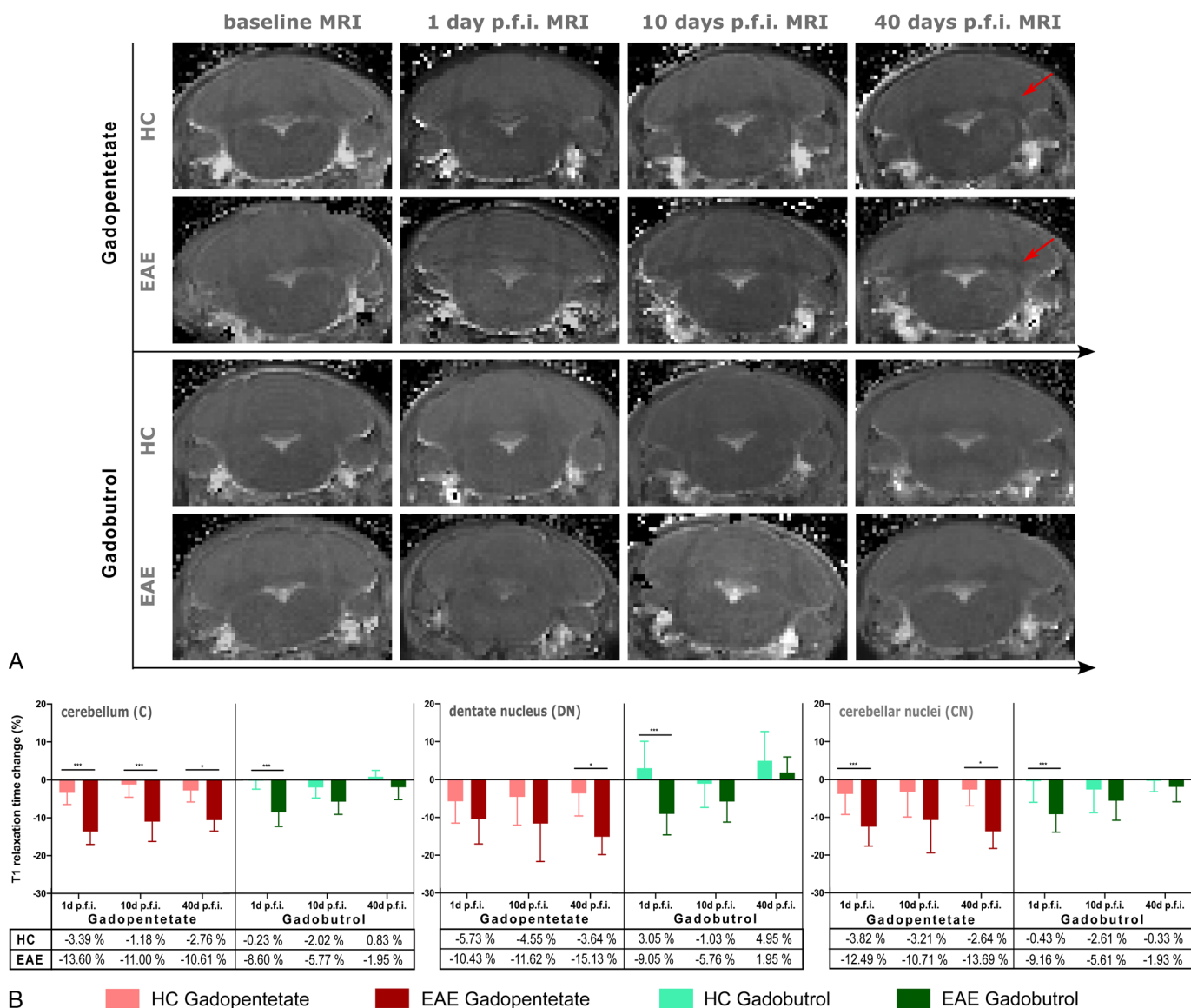
**FIGURE 3.** 7 T MRI relaxometry in vivo. A, Representative longitudinal MRI scans (T1 map RARE-VTR sequence) of animals sacrificed 40 days pfi of GBCAs. Relaxometry revealed decreasing T1 relaxation times within the CN (red arrow) toward day 40 pfi of gadopentetate in EAE and HC animals. Gadobutrol-treated animals did not show prominent qualitative T1 shortening within the CN. B, T1 relaxation time change (%) differences between EAE and HC animals within the C, DN, and CN for both tested GBCAs. Mann-Whitney tests were computed for EAE versus HC after gadopentetate or gadobutrol treatment and the Bonferroni correction was applied for multiple testing over 3 consecutive time points. Data are displayed as mean ± SD.

levels were detected in all blood samples at all analyzed time points pfi of both GBCAs, gadopentetate and gadobutrol (supplementary Figure SDC 2B, http://links.lww.com/RLI/A704). In line with Gd content within cerebellar brain slices assessed using LA-ICP-MS, EAE animals showed elevated Gd levels compared with HC animals (except at day 10 pfi of gadopentetate). Maximal Gd concentrations detected corresponded to 0.0054% of the intravenously injected cumulative dose of 20 mmol/kg BW (24 hours pfi of gadopentetate in EAE mice). A negative control sample (untreated age- and sex-matched mouse) demonstrated a very low Gd concentration of 0.0002 μg/g, as shown in the supplementary Figure SDC 2B, http://links.lww.com/RLI/A704. Because of the low sample size (n = 2 per group; HC at day 1 pfi of gadopentetate: n = 1 due to sample contamination) and high variation, only descriptive statistics were performed (see Supplemental Digital Content, Figure SDC 2B, http://links.lww.com/RLI/A704).

LA-ICP-MS Revealed Elevated Zinc Content in Inflamed Mouse Brains

Next, we aimed to identify endogenous metals whose distribution may be affected by inflammation and could be related to Gd retention within cerebellar structures. Interestingly, elevated Zn levels were found in cerebellar slices of EAE animals compared with HC mice at all time points, irrespective of the applied GBCA (Fig. 5A, B). Zn was diffusely distributed in the EAE cerebellar sections at 24 hours pfi of GBCAs, whereas 10 and 40 days pfi, high Zn levels were predominantly located within and around the CN within the white matter and layers of the cerebellar cortex (Fig. 5A). Furthermore, cerebellar EAE slices, as well as HC slices, revealed a decreasing trend in Zn levels toward day 40 pfi. This trend was particularly pronounced in the inflamed DN and CN, irrespective of the applied GBCA, as shown in Figure 5B. Amounts of Zn in
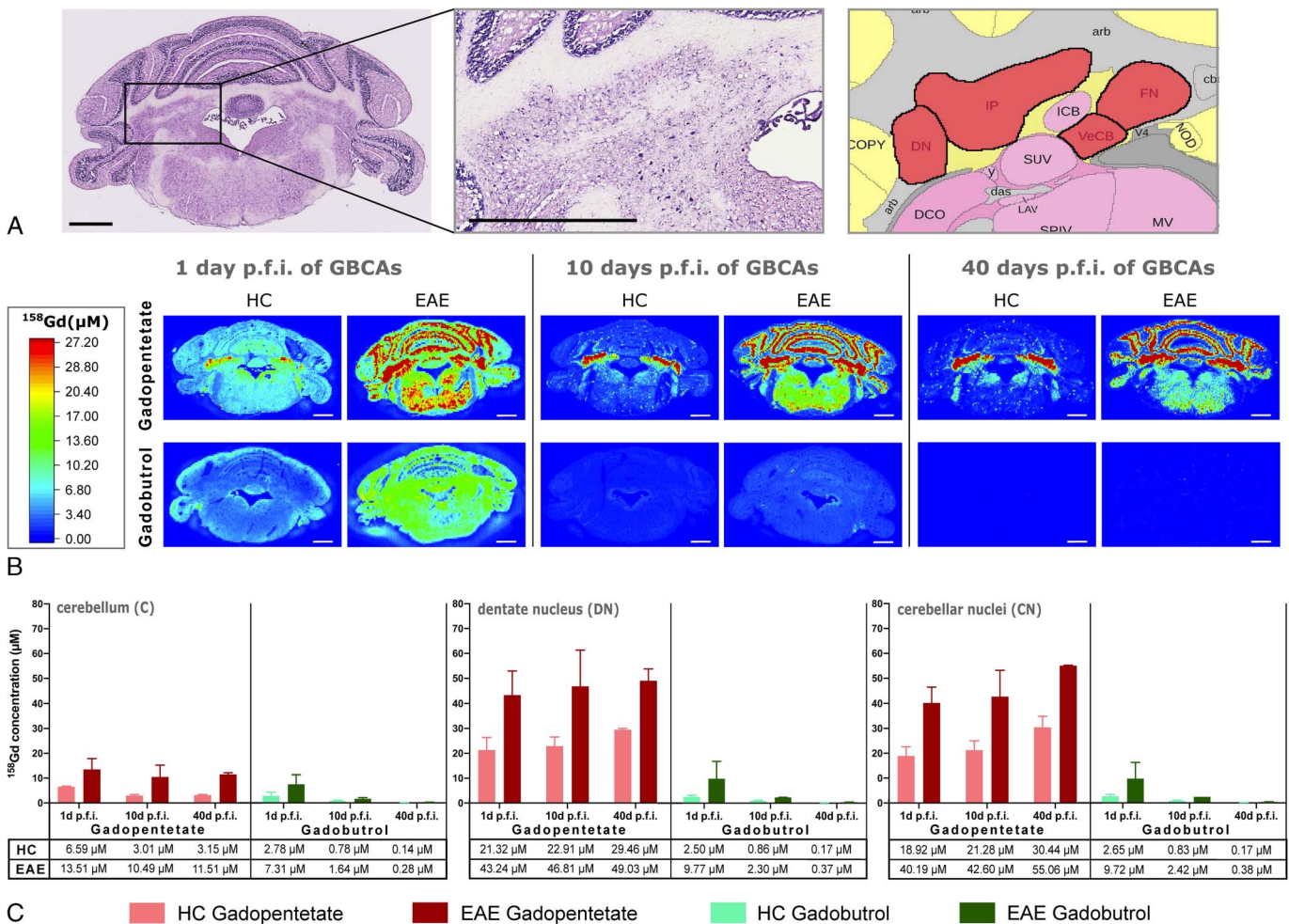
FIGURE 4. Analysis of Gd distribution using LA-ICP-MS. A, On the left, H&E bright field image of cerebellar slice containing the CN corresponding to LA-ICP-MS tissue layer at ×2 magnification; CNs are additionally displayed at ×10 magnification. On the right, Allen brain atlas correlation image of CN formation. Nuclei from lateral to medial: DN, interposed nucleus (IP), vestibulocerebellar nucleus (VeCB), fastigial nucleus (FN). Scale bars: 1 mm. B, LA-ICP-MS images showing Gd distribution in cerebellar slices. Red areas display high and blue areas low Gd content (μM). Scale bars: 1 mm. C, Gd concentrations measured within the whole C, DN, or CN in μM of brain volume. Because of the low sample size, merely descriptive statistics are shown (mean ± SD).

EAE brains regarding the C, DN, and CN decreased by 25%, 26%, and 26%, respectively, whereas in HC brains, Zn levels decreased by 14%, 21%, and 22%, respectively, toward day 40 pfi (Fig. 5B).

The overall distribution of Cu, Ca, P, S, Mn, and Fe concentrations seemed to be unaffected by inflammation (supplementary Figure SDC 3, http://links.lww.com/RLI/A705). However, areas with high Gd content overlapped with areas of high Fe levels (see Supplemental Digital Content, Figure SDC 3, http://links.lww.com/RLI/A705).

Gadopentetate but Not Gadobutrol Exerts a Neurotoxic Effect on Living Organotypic Hippocampal Slices

To assess the potential toxicity of GBCAs, we measured the cell death rate (%) after 48-hour treatment of chronic hippocampal slices with gadopentetate or gadobutrol at 1, 10, and 50 mM, respectively (Fig. 6). To simulate neuroinflammatory conditions, TNF-α at 50 ng/mL was added to half of the slices. Gadopentetate promoted cell death within the DG only at 50 mM (Fig. 6A, B). No toxicity was observed for gadobutrol. Tumor necrosis factor α at 50 ng/mL enhanced the gadopentetate-induced cell death rate significantly (with vs without TNF-α: 3.15% ± 01.18% vs 2.17% ± 1.14%; $P = 0.0345$), as shown in

Figure 6B. NMDA incubation at 50 μM served as a positive control. Its neurotoxic effect was also increased by TNF-α (34.34% ± 11.14% vs 19.70% ± 9.19%; $P = 0.0002$) (Fig. 6B).

To examine whether the lack of cytotoxicity of GBCAs at especially lower concentrations was caused by deficient penetration of the compounds into the living slices, IMC was performed using slices treated with 10 mM of GBCAs. Gadolinium was detectable inside hippocampal slices after treatment with both GBCAs, gadopentetate and gadobutrol (Fig. 6C). However, the mean [158]Gd count inside the DG region was 26 times higher in slices treated with gadopentetate than in those treated with gadobutrol (6.07 ± 1.32 ion count vs 0.23 ± 0.02 ion count). Nevertheless, the mean ion count for [158]Gd within the gadobutrol-treated slices was still on average 12 times higher compared with untreated control slices (0.23 ± 0.02 ion count vs 0.02 ± 0.01 ion count). Interestingly, in gadopentetate-treated slices, detected [191, 193]Ir (labels nucleic acids) colocalized with areas of high [158]Gd counts within the DG (Fig. 6C).

DISCUSSION

We demonstrated previously that after repeated applications of gadopentetate, neuroinflammation favors the retention of Gd within
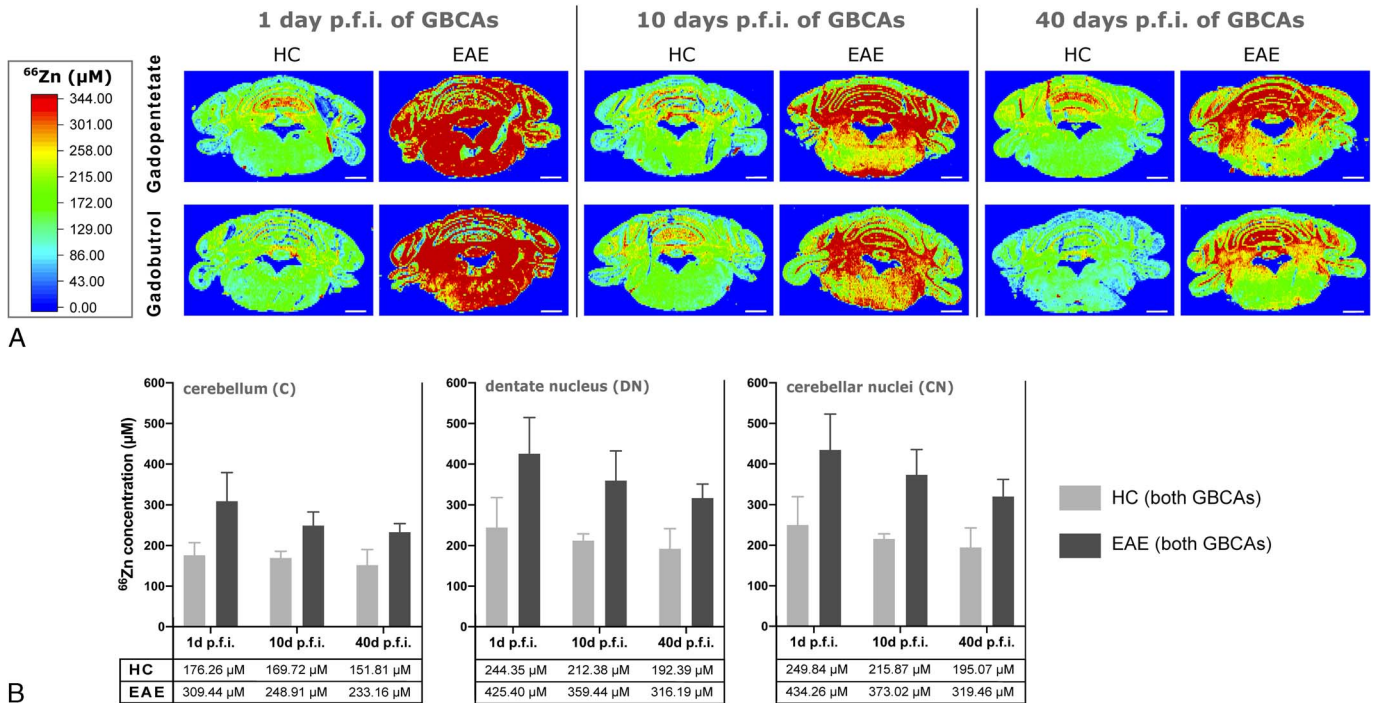
FIGURE 5. Analysis of elemental colocalization using LA-ICP-MS. A, Laser ablation images of cerebellar Zn distribution. Red areas display high and blue areas low Zn content (μM). The EAE animals in both GBCA groups showed qualitatively higher Zn levels compared with HC. Scale bars: 1 mm. B, Demonstration of Zn levels within the whole C, the DN, and CN (μM). The EAE animals consistently presented higher elemental Zn levels than HC animals irrespective of the applied GBCA with a tendency to decrease toward day 40 pfi of GBCAs.

the CNS in vivo.[37] Here, in a murine model of multiple sclerosis as well as in living brain tissue, we compared the linear gadopentetate and the macrocyclic gadobutrol in terms of dynamics and patterns of inflammation-promoted Gd retention in vivo as well as potential cytotoxic effects ex vivo. Using T1 relaxometry and LA-ICP-MS, we found that gadopentetate was retained in the brain up to 40 days pfi, whereas gadobutrol was efficiently washed out toward day 40 pfi. Although for both GBCAs inflammation favored enhanced Gd retention within cerebellar structures, gadopentetate led to much larger Gd brain retention compared with gadobutrol. Finally, using an ex vivo model of neuronal tissue, we showed that gadopentetate but not gadobutrol induced cell death in the living brain tissue and that this process was enhanced in the presence of the inflammatory mediator TNF-α.

Our study revealed significantly decreased T1 relaxation times after multiple injections of GBCAs in EAE brains compared with HC. T1 relaxometry is a robust tool to study MRI alterations related to Gd retention after administration of GBCAs in a quantitative manner,[42,43] without the need for a reference region, which in itself may be a confounding factor.[13,44] Using the well-established ABA registration tool, we chose an automated approach to identify T1 relaxation decreases within different brain areas, ensuring higher validity and comparability. The LA-ICP-MS data confirmed the relaxometry findings, as cerebellar Gd levels in EAE mice were 2- to 3-fold higher than in HC mice and within the range previously reported by us and others.[15,37,45] Maximal Gd contents inside the CN and DN after repeated injections of gadopentetate corresponded to approximately 4.51 μg/g in HC mice and 8.28 μg/g in EAE mice (30 μM and 55 μM, respectively).

Comparing the 2 applied GBCAs overtime, LA-ICP-MS data confirmed that neuroinflammation enhanced Gd retention especially after gadopentetate administration. We observed a long-term retention in the EAE cerebellum and its nuclei, and to a lower extent also in HC brains, up to 40 days pfi of the linear compound. However, gadobutrol administration led to a rather low and transient retention of Gd until day 10 pfi, which was also enhanced during inflammation but was completely

cleared from the brain at day 40 pfi. Recent studies demonstrated a nonpermanent retention of macrocyclic GBCAs[33,34,46,47] with clearance rates dependent on the specific washout kinetics.[33,34] Frenzel et al suggested that gadobutrol remained in its intact form inside the body as it was exclusively present in the soluble fraction of the brain as a low-molecular-weight molecule. In contrast, linear GBCAs at day 24 pfi were present to a large extent in an insoluble form, whereas in its soluble fraction, a portion of Gd was bound to large macromolecules, suggesting that Gd had dissociated from the chelate.[15] These findings were confirmed in recent rodent studies.[45,48,49]

We speculate that BBB disruption[37] and/or alterations of the choroid plexus[50] occurring during EAE contribute to the enhanced entry of GBCA into the brain, whereas inflammation-mediated tissue alterations[51–54] may promote enhanced Gd retention. In healthy individuals, Gd retention inside the brain seems to be the result of an entry of GBCA through the blood-CSF barrier[55] at the choroid plexus and from the CSF via the glymphatic system,[56–59] into the brain. Along these lines, Öner et al[60] reported on DN T1 hyperintensities after only a single intrathecal injection of gadopentetate in patients with normal renal function. It has been shown that alterations of the choroid plexus observed in multiple sclerosis[61] and EAE[62] may contribute to CNS pathology. Thus, an enhanced entry of GBCA into the CSF via the inflamed choroid plexus could be assumed.

Moreover, BBB breakdown is considered an early hallmark in multiple sclerosis that permits large CNS infiltration of peripheral activated autoreactive lymphocytes into the CNS. In addition, inflammation-related release of chemokines, free radicals, activated matrix metalloproteinases (MMP) and the consequent enhanced extravasation of immune cells may further compromise BBB integrity.[63] Blood-brain barrier disruption occurs in a similar way in the EAE model, in which T lymphocytes have been demonstrated to induce tight junction alterations in BBB endothelium initiating barrier disruption and enhanced permeability.[64,65] Whereas a leaky BBB may result in elevated GBCA diffusion, additional cellular and tissue
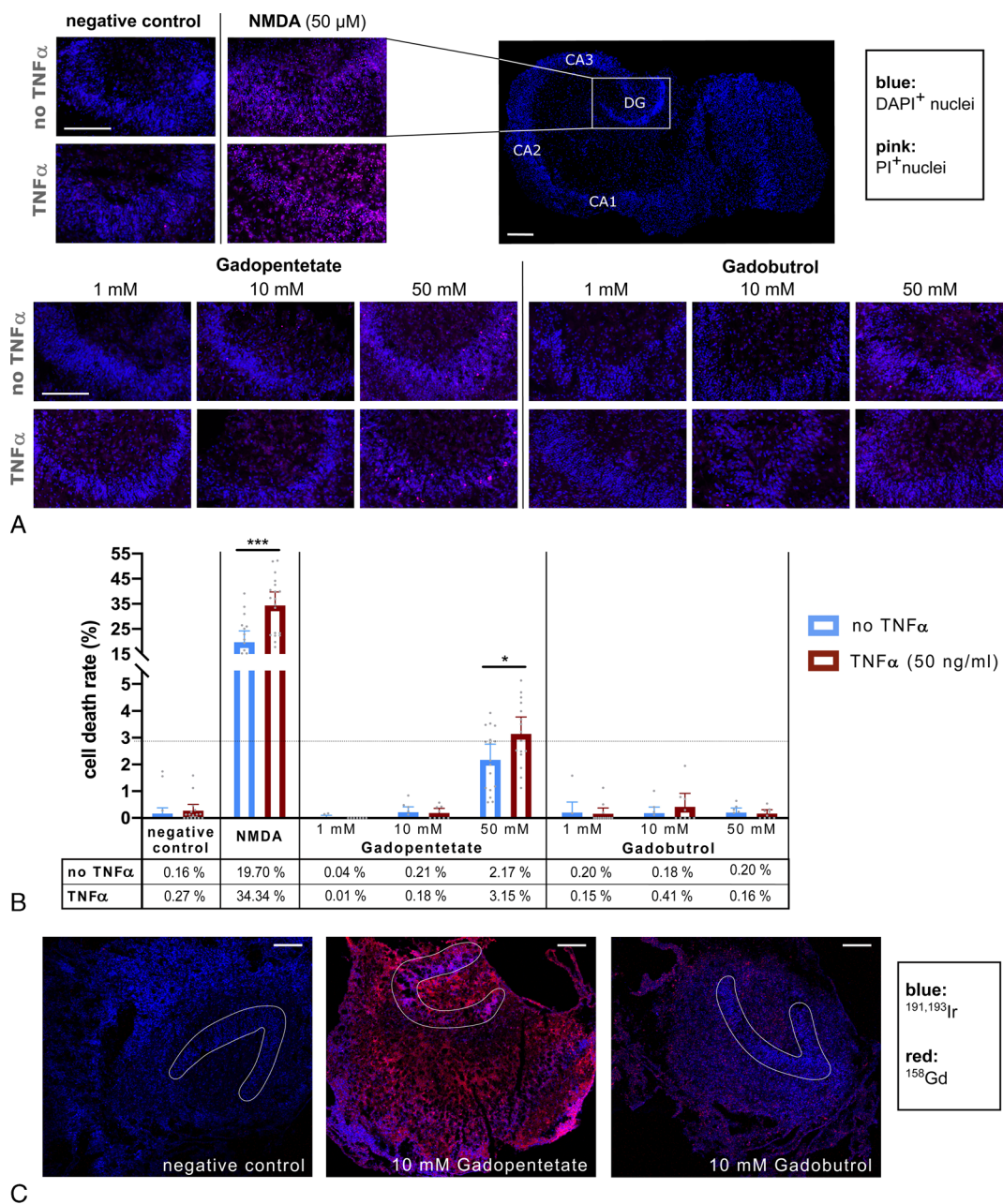
FIGURE 6. Toxicity of GBCAs on organotypic hippocampal slices. A, Representative fluorescence images of the DG; all nuclei in blue (DAPI), dead nuclei in red (PI). The DGs of slices coincubated with/without TNF-α (50 ng/mL) are displayed for all experimental conditions. The PI-positive cells appear in NMDA-treated (±TNF-α) and gadopentetate-treated slices at 50 mM (±TNF-α). Scale bars: 200 μm. B, Cell death rate (%) was elevated in NMDA (positive control)-treated slices and slices treated with 50 mM gadopentetate. Tumor necrosis factor α enhanced cell death rate significantly. Data were evaluated using Mann-Whitney tests (mean ± SD). C, IMC images of 10-μm-thick slices after gadopentetate or gadobutrol treatment at 10 mM and negative control. The DGs were surrounded by manually drawn ROIs (white), and thresholds were adjusted for optimal visualization. Scale bars: 200 μm.

alterations such as demyelination, microglial activation, changes in elemental metal distribution, or/and alterations of the extracellular matrix may contribute to enhanced retention. In this context, it has been suggested that inflammation-mediated alterations in the extracellular matrix composition such as glycosaminoglycans (GAGs) may favor GBCA dechelation and parenchymal retention of Gd.[37] We previously reported that in EAE, inflammation-induced modifications of GAG sulfation on brain endothelial cells facilitate the uptake of very small superparamagnetic iron oxide nanoparticles.[51] The GAG network on endothelial cells of vessels may act as an ion exchanger with complexing abilities.[66] Interestingly, the DN was found to contain elevated amounts of microvessels that may bind Gd[23] and to be enriched in endogenous metals such as Fe, Cu, and Zn that may facilitate transmetallation processes.[67]

Strikingly, we observed increasing Gd levels within the CN (DN included) from day 10 to day 40 pfi, which was observed also in HC but was more pronounced in the EAE animals. We speculate that this increase over time within the CN on day 10 and 40 pfi may be the result of a release of Gd^{3+} from other storage organs such as the bones.[3,68–70]

Stable Gd retention inside the bone has been reported for a period of more than 8 years most likely caused by the transmetallation of Gd^{3+} with resident calcium ions.[69,71] Thakral and Abraham[72] reported on increasing Gd amounts in sequential skin biopsies of patients with nephrogenic systemic fibrosis although no more GBCA was administered. Bone storage may also contribute to maintain Gd tissue levels by its mobilization into the bloodstream, since it was reported that Gd was still detectable in the red blood cell compartment 10 days pfi of principally linear GBCAs.[18] Our ICP-MS analysis of blood samples revealed indeed that Gd was present in all samples up to day 40 pfi within the same range as detected in the cerebellum (approximately 0.2–2.0 µg/g). This supports the hypothesis of long-term retention, release, and recirculation of Gd through the body according to the Le Chatelier principle.[73]

We also showed that Zn levels in EAE brains were elevated compared with HC brains irrespective of the administered GBCA at all investigated time points. It has been suggested that disruption of brain Zn homeostasis may play an active role in the pathogenesis of multiple sclerosis and EAE.[74,75] Zn acts as a cofactor for numerous enzymes like MMPs, is component of various proteins including myelin basic protein,[74] and was reported to induce mitochondrial production of reactive oxygen species.[75] Hence, increased neuronal Zn release may lead to MMP activation compromising BBB integrity and mediate neuronal injury. In this line, Choi et al[75] reported on decreased BBB impairment and reduced immune cell infiltration and myelin destruction in the spinal cord of EAE mice after oral zinc chelator application.

We further observed that cerebellar Zn concentrations decreased until day 40 pfi, whereas Gd levels increased. Several studies reported on Zn depletion due to transmetallation with Gd and resulting zincuria after injections of linear GBCAs.[31,76,77] Thus, increased Zn content in EAE brains may lead to elevated transmetallation rates with administered Gd and therefore facilitate its retention.

Furthermore, we investigated how GBCAs may affect cell viability using a model of organotypic hippocampal slice cultures in which the 3-dimensional histological architecture and cellular composition of neuronal tissue are well preserved.[78] We demonstrated that tissue retention of Gd was 26-fold higher after gadopentetate incubation compared with gadobutrol as measured by IMC and that gadopentetate induced neural death. Preincubation and coincubation of chronic hippocampal cultures with TNF-α at 50 ng/mL increased cell death induced by gadopentetate but did not influence gadobutrol effects. This finding underlines the hypothesis that not only an impaired BBB but also tissue alterations attributable to a proinflammatory milieu may cause elevated Gd retention in the CNS. Tumor necrosis factor α is a pleiotropic cytokine playing an essential role in the immunopathogenesis of multiple sclerosis and EAE[64] that is widely used in in vitro paradigms of inflammation.[51] In our ex vivo model, TNF-α may increase GBCA toxicity by enhancing cell death–inducing pathways as part of its immunomodulatory capacity.[64,79] However, it cannot be excluded that TNF-α triggers a decreased chelate stability owing to changes in endogenous ions resulting in a dose-dependent increase in GBCA-induced toxicity.[80] Our findings are consistent with a recent study that demonstrated toxicity for linear GBCAs in vitro in human dopaminergic neurons.[81] Moreover, Xia et al[82] observed that Gd chloride (20 µM) reduced cell viability and led to rapid accumulation of intracellular calcium and reactive oxygen species. However, the in vivo relevance of those findings remains unclear. Whereas Radbruch et al[83] reported on reduced intraepidermal nerve fiber density in mice after a single application of linear GBCAs and to a lesser extent after macrocyclic GBCAs, Davies et al, among others,[19,25,84,85] did not detect any histopathological changes suggestive of neurotoxicity in rat tissue after multiple injections of gadodiamide. Furthermore, in vivo administration of gadodiamide did not lead to persistent clinical and behavioral alterations in healthy rats.[85] Nevertheless, further investigations on the genotoxic potential of GBCAs are needed, as Gd retention was found inside nuclei of neuronal cells.[22] Our IMC measurements showed that Gd retained inside the DG was colocalized with Ir-tagged nucleic acids.

However, because of limited image resolution, we were not able to differentiate between an intracellular or extracellular location of retained Gd.

It is uncertain whether Gd retention may promote neuronal alterations in vivo and lead, for instance, to additional clinical impairment in patients with multiple sclerosis.[42,86–89] Only a few studies reported an increase in clinical disability after GBCA administration.[42,88] Further investigations are needed to determine to what extent parenchymal retention of potentially dissociating and, hence, toxic Gd^{3+} represents a long-term hazard in particular for patients with neuroinflammatory diseases.

Limitations of the Study

Although the EAE recapitulates many of the pathological hallmarks of multiple sclerosis, the pattern of GBCA administration (8 injections in 10 days), the high dosage (single daily dose of 2.5 mmol/kg BW), and the time points selected for long-term measures (up to 40 days pfi of GBCAs) represent a well-established rodent paradigm[16,17,25,37,90] but differ considerably from the reality in patients in terms of concentrations and time frame of the applications. Moreover, the sample size of n = 2 animals per group for LA-ICP-MS measurements was too small to make any quantitative statement about Gd retention but did show obvious and consistent qualitative trends in EAE versus HC animals. In addition, we did not conduct any structural analysis on Gd retained in the tissue and cannot distinguish between intact GBCA, free Gd^{3+}, and Gd bound in insoluble deposits or to soluble macromolecules. Further studies are currently ongoing to clarify this important issue. Finally, using the technique of chronic slice culture for toxicity assessment, initially applied GBCA concentrations ex vivo were approximately 1000-fold higher than Gd concentrations identified inside the CN and DN in vivo using LA-ICP-MS. However, we were not able to determine the specific gadopentetate concentration that infiltrated the chronic tissue slices and consequently led to neuronal cell death within the DG or the mechanisms, leading to increased cell death with simultaneous TNF-α incubation. This should be also assessed in future studies. Furthermore, because of fixation and staining procedures on hippocampal slices, a partial washout of intact GBCA cannot be excluded. Nevertheless, we here aimed to assess tissue-bound Gd potentially leading to neurotoxicity of DG neuronal cells rather than measuring additional intact GBCA amounts.

CONCLUSIONS

Using in vivo MRI and LA-ICP-MS, we studied the effect of inflammation on the long-term retention and cerebellar distribution of Gd after repeated administration of linear gadopentetate and macrocyclic gadobutrol. The kinetics of Gd retention and ICP-MS analysis of blood samples indicated that Gd from gadopentetate may be stored in nonneuronal tissue and recirculated through the body for a long time after the last GBCA application. In addition, regarding gadobutrol, we showed that inflammation led to a nonpermanent Gd retention most likely owing to an increased influx into the cerebellum of EAE mice, which was efficiently cleared over time. Finally, using living brain tissue, we demonstrated that gadopentetate but not gadobutrol induced cell death within the chronic hippocampal slices; a process that was also increased in an inflammatory milieu. Thus, our study confirmed the higher kinetic stability of macrocyclic GBCAs compared with the linear compounds in vivo. Although macrocyclic GBCAs do not seem to cause long-term Gd retention either in inflamed or in healthy brain parenchyma, there is a substantial need to elucidate the mechanisms causing enhanced retention inside inflamed brain parenchyma and to determine if even transient short-term Gd retention after the use of kinetically more stable agents may exert toxic effects on inflamed brain tissue in vivo.

REFERENCES

1. Hao D, Ai T, Goerner F, et al. MRI contrast agents: basic chemistry and safety. *J Magn Reson Imaging*. 2012;36:1060–1071.

2. Do QN, Lenkinski RE, Tircso G, et al. How the chemical properties of GBCAs influence their safety profiles in vivo. *Molecules*. 2021;27:58.

3. Runge VM. Dechelation (transmetalation): consequences and safety concerns with the linear gadolinium-based contrast agents, in view of recent health care rulings by the EMA (Europe), FDA (United States), and PMDA (Japan). *Invest Radiol*. 2018;53:571–578.

4. European Medicines Agency. EMA's final opinion confirms restrictions on use of linear gadolinium agents in body scan. 2017. https://www.ema.europa.eu/en/news/emas-final-opinion-confirms-restrictions-use-linear-gadolinium-agents-body-scans. Assessed March 2, 2022.

5. US Food and Drug Administration. FDA warns that gadolinium-based contrast agents (GBCAs) are retained in the body; requires new class warnings. 2017. https://www.fda.gov/drugs/drug-safety-and-availability/fda-drug-safety-communication-fda-warns-gadolinium-based-contrast-agents-gbcas-are-retained-body. Accessed March 2, 2022.

6. Kanda T, Ishii K, Kawaguchi H, et al. High signal intensity in the dentate nucleus and globus pallidus on unenhanced T1-weighted MR images: relationship with increasing cumulative dose of a gadolinium-based contrast material. *Radiology*. 2014;270:834–841.

7. Errante Y, Cirimele V, Mallio CA, et al. Progressive increase of T1 signal intensity of the dentate nucleus on unenhanced magnetic resonance images is associated with cumulative doses of intravenously administered gadodiamide in patients with normal renal function, suggesting dechelation. *Invest Radiol*. 2014;49:685–690.

8. Quattrocchi CC, Mallio CA, Errante Y, et al. Gadodiamide and dentate nucleus T1 hyperintensity in patients with meningioma evaluated by multiple follow-up contrast-enhanced magnetic resonance examinations with no systemic interval therapy. *Invest Radiol*. 2015;50:470–472.

9. Radbruch A, Weberling LD, Kieslich PJ, et al. High-signal intensity in the dentate nucleus and globus pallidus on unenhanced T1-weighted images: evaluation of the macrocyclic gadolinium-based contrast agent gadobutrol. *Invest Radiol*. 2015;50:805–810.

10. Weberling LD, Kieslich PJ, Kickingereder P, et al. Increased signal intensity in the dentate nucleus on unenhanced T1-weighted images after gadobenate dimeglumine administration. *Invest Radiol*. 2015;50:743–748.

11. Ramalho J, Castillo M, AlObaidy M, et al. High signal intensity in globus pallidus and dentate nucleus on unenhanced T1-weighted MR images: evaluation of two linear gadolinium-based contrast agents. *Radiology*. 2015;276:836–844.

12. Cao Y, Huang DQ, Shih G, et al. Signal change in the dentate nucleus on T1-weighted MR images after multiple administrations of gadopentetate dimeglumine versus gadobutrol. *AJR Am J Roentgenol*. 2016;206:414–419.

13. Robert P, Lehericy S, Grand S, et al. T1-weighted hypersignal in the deep cerebellar nuclei after repeated administrations of gadolinium-based contrast agents in healthy rats: difference between linear and macrocyclic agents. *Invest Radiol*. 2015;50:473–480.

14. Robert P, Violas X, Grand S, et al. Linear gadolinium-based contrast agents are associated with brain gadolinium retention in healthy rats. *Invest Radiol*. 2016;51:73–82.

15. Frenzel T, Apte C, Jost G, et al. Quantification and assessment of the chemical form of residual gadolinium in the brain after repeated administration of gadolinium-based contrast agents: comparative study in rats. *Invest Radiol*. 2017;52:396–404.

16. Lohrke J, Frisk AL, Frenzel T, et al. Histology and gadolinium distribution in the rodent brain after the administration of cumulative high doses of linear and macrocyclic gadolinium-based contrast agents. *Invest Radiol*. 2017;52:324–333.

17. Jost G, Frenzel T, Boyken J, et al. Long-term excretion of gadolinium-based contrast agents: linear versus macrocyclic agents in an experimental rat model. *Radiology*. 2019;290:340–348.

18. Di Gregorio E, Furlan C, Atlante S, et al. Gadolinium retention in erythrocytes and leukocytes from human and murine blood upon treatment with gadolinium-based contrast agents for magnetic resonance imaging. *Invest Radiol*. 2020;55:30–37.

19. Davies J, Marino M, Smith APL, et al. Repeat and single dose administration of gadodiamide to rats to investigate concentration and location of gadolinium and the cell ultrastructure. *Sci Rep*. 2021;11:13950.

20. McDonald RJ, McDonald JS, Kallmes DF, et al. Intracranial gadolinium deposition after contrast-enhanced MR imaging. *Radiology*. 2015;275:772–782.

21. Kanda T, Fukusato T, Matsuda M, et al. Gadolinium-based contrast agent accumulates in the brain even in subjects without severe renal dysfunction: evaluation of autopsy brain specimens with inductively coupled plasma mass spectroscopy. *Radiology*. 2015;276:228–232.

22. McDonald RJ, McDonald JS, Kallmes DF, et al. Gadolinium deposition in human brain tissues after contrast-enhanced MR imaging in adult patients without intracranial abnormalities. *Radiology*. 2017;285:546–554.

23. Fingerhut S, Sperling M, Holling M, et al. Gadolinium-based contrast agents induce gadolinium deposits in cerebral vessel walls, while the neuropil is not affected: an autopsy study. *Acta Neuropathol*. 2018;136:127–138.

24. El-Khatib AH, Radbruch H, Trog S, et al. Gadolinium in human brain sections and colocalization with other elements. *Neurol Neuroimmunol Neuroinflamm*. 2019;6:e515.

25. El Hamrani D, Vives V, Buchholz R, et al. Effect of long-term retention of gadolinium on metabolism of deep cerebellar nuclei after repeated injections of gadodiamide in rats. *Invest Radiol*. 2020;55:120–128.

26. Radbruch A, Richter H, Fingerhut S, et al. Gadolinium deposition in the brain in a large animal model: comparison of linear and macrocyclic gadolinium-based contrast agents. *Invest Radiol*. 2019;54:531–536.

27. Frenzel T, Lengsfeld P, Schirmer H, et al. Stability of gadolinium-based magnetic resonance imaging contrast agents in human serum at 37 degrees C. *Invest Radiol*. 2008;43:817–828.

28. Port M, Idee JM, Medina C, et al. Efficiency, thermodynamic and kinetic stability of marketed gadolinium chelates and their possible clinical consequences: a critical review. *Biometals*. 2008;21:469–490.

29. Idée JM, Port M, Raynal I, et al. Clinical and biological consequences of transmetallation induced by contrast agents for magnetic resonance imaging: a review. *Fundam Clin Pharmacol*. 2006;20:563–576.

30. Telgmann L, Wehe CA, Kunnemeyer J, et al. Speciation of Gd-based MRI contrast agents and potential products of transmetalation with iron ions or parenteral iron supplements. *Anal Bioanal Chem*. 2012;404:2133–2141.

31. Boyken J, Frenzel T, Lohrke J, et al. Impact of treatment with chelating agents depends on the stability of administered GBCAs: a comparative study in rats. *Invest Radiol*. 2019;54:76–82.

32. Robert P, Fingerhut S, Factor C, et al. One-year retention of gadolinium in the brain: comparison of gadodiamide and gadoterate meglumine in a rodent model. *Radiology*. 2018;288:424–433.

33. Bussi S, Coppo A, Botteron C, et al. Differences in gadolinium retention after repeated injections of macrocyclic MR contrast agents to rats. *J Magn Reson Imaging*. 2018;47:746–752.

34. Bussi S, Coppo A, Celeste R, et al. Macrocyclic MR contrast agents: evaluation of multiple-organ gadolinium retention in healthy rats. *Insights Imaging*. 2020;11:11.

35. Giorgio A, De Stefano N. Effective utilization of MRI in the diagnosis and management of multiple sclerosis. *Neurol Clin*. 2018;36:27–34.

36. Wattjes MP, Ciccarelli O, Reich DS, et al. 2021 MAGNIMS-CMSC-NAIMS consensus recommendations on the use of MRI in patients with multiple sclerosis. *Lancet Neurol*. 2021;20:653–670.

37. Wang S, Hesse B, Roman M, et al. Increased retention of gadolinium in the inflamed brain after repeated administration of gadopentetate dimeglumine: a proof-of-concept study in mice combining ICP-MS and micro- and nano-SR-XRF. *Invest Radiol*. 2019;54:617–626.

38. Koch S, Mueller S, Foddis M, et al. Atlas registration for edema-corrected MRI lesion volume in mouse stroke models. *J Cereb Blood Flow Metab*. 2019;39:313–323.

39. Stärk HJ, Wennrich R. A new approach for calibration of laser ablation inductively coupled plasma mass spectrometry using thin layers of spiked agarose gels as references. *Anal Bioanal Chem*. 2011;399:2211–2217.

40. Schneider CA, Rasband WS, Eliceiri KW. NIH image to ImageJ: 25 years of image analysis. *Nat Methods*. 2012;9:671–675.

41. Opitz-Araya X, Barria A. Organotypic hippocampal slice cultures. *J Vis Exp*. 2011;2462.

42. Forslin Y, Martola J, Bergendal Å, et al. Gadolinium retention in the brain: an MRI relaxometry study of linear and macrocyclic gadolinium-based contrast agents in multiple sclerosis. *AJNR Am J Neuroradiol*. 2019;40:1265–1273.

43. Deike-Hofmann K, Reuter J, Haase R, et al. No changes in T1 relaxometry after a mean of 11 administrations of gadobutrol. *Invest Radiol*. 2020;55:381–386.

44. Jost G, Lenhard DC, Sieber MA, et al. Signal increase on unenhanced T1-weighted images in the rat brain after repeated, extended doses of gadolinium-based contrast agents: comparison of linear and macrocyclic agents. *Invest Radiol*. 2016;51:83–89.

45. Strzeminska I, Factor C, Jimenez-Lamana J, et al. Comprehensive speciation analysis of residual gadolinium in deep cerebellar nuclei in rats repeatedly administered with gadoterate meglumine or gadodiamide [published online ahead of print January 19, 2022]. *Invest Radiol*. doi:10.1097/RLI.0000000000000846.

46. Frenzel T, Ulbrich HF, Pietsch H. The macrocyclic gadolinium-based contrast agents gadobutrol and gadoteridol show similar elimination kinetics from the brain after repeated intravenous injections in rabbits. *Invest Radiol*. 2021;56:341–347.

47. Strzeminska I, Factor C, Robert P, et al. Long-term evaluation of gadolinium retention in rat brain after single injection of a clinically relevant dose of gadolinium-based contrast agents. *Invest Radiol*. 2020;55:138–143.

48. Gianolio E, Bardini P, Arena F, et al. Gadolinium retention in the rat brain: assessment of the amounts of insoluble gadolinium-containing species and intact gadolinium complexes after repeated administration of gadolinium-based contrast agents. *Radiology*. 2017;285:839–849.

49. Strzeminska I, Factor C, Robert P, et al. Speciation analysis of gadolinium in the water-insoluble rat brain fraction after administration of gadolinium-based contrast agents. *Invest Radiol*. 2021;56:535–544.

50. Millward JM, Schnorr J, Taupitz M, et al. Iron oxide magnetic nanoparticles highlight early involvement of the choroid plexus in central nervous system inflammation. *ASN Neuro*. 2013;5:e00110.

51. Berndt D, Millward JM, Schnorr J, et al. Inflammation-induced brain endothelial activation leads to uptake of electrostatically stabilized iron oxide nanoparticles via sulfated glycosaminoglycans. *Nanomedicine*. 2017;13:1411–1421.

52. Millward JM, Ariza de Schellenberger A, Berndt D, et al. Application of europium-doped very small Iron oxide nanoparticles to visualize Neuroinflammation with MRI and fluorescence microscopy. *Neuroscience*. 2019;403:136–144.

53. Silva RV, Morr AS, Mueller S, et al. Contribution of tissue inflammation and blood-brain barrier disruption to brain softening in a mouse model of multiple sclerosis. *Front Neurosci*. 2021;15:701308.

54. Wang S, Millward JM, Hanke-Vela L, et al. MR elastography-based assessment of matrix remodeling at lesion sites associated with clinical severity in a model of multiple sclerosis. *Front Neurol*. 2020;10:1382.

55. Jost G, Frenzel T, Lohrke J, et al. Penetration and distribution of gadolinium-based contrast agents into the cerebrospinal fluid in healthy rats: a potential pathway of entry into the brain tissue. *Eur Radiol*. 2017;27:2877–2885.

56. Rasschaert M, Idée JM, Robert P, et al. Moderate renal failure accentuates T1 signal enhancement in the deep cerebellar nuclei of gadodiamide-treated rats. *Invest Radiol*. 2017;52:255–264.

57. Taoka T, Naganawa S. Gadolinium-based contrast media, cerebrospinal fluid and the glymphatic system: possible mechanisms for the deposition of gadolinium in the brain. *Magn Reson Med Sci*. 2018;17:111–119.

58. Nehra AK, McDonald RJ, Bluhm AM, et al. Accumulation of gadolinium in human cerebrospinal fluid after gadobutrol-enhanced MR imaging: a prospective observational cohort study. *Radiology*. 2018;288:416–423.

59. Rasschaert M, Schroeder JA, Wu TD, et al. Multimodal imaging study of gadolinium presence in rat cerebellum: differences between Gd chelates, presence in the Virchow-Robin space, association with lipofuscin, and hypotheses about distribution pathway. *Invest Radiol*. 2018;53:518–528.

60. Öner AY, Barutcu B, Aykol Ş, et al. Intrathecal contrast-enhanced magnetic resonance imaging-related brain signal changes: residual gadolinium deposition? *Invest Radiol*. 2017;52:195–197.

61. Solár P, Zamani A, Kubíčková L, et al. Choroid plexus and the blood-cerebrospinal fluid barrier in disease. *Fluids Barriers CNS*. 2020;17:35.

62. Engelhardt B, Wolburg-Buchholz K, Wolburg H. Involvement of the choroid plexus in central nervous system inflammation. *Microsc Res Tech*. 2001;52:112–129.

63. Balasa R, Barcutean L, Mosora O, et al. Reviewing the significance of blood-brain barrier disruption in multiple sclerosis pathology and treatment. *Int J Mol Sci*. 2021;22:8370.

64. Fresegna D, Bullitta S, Musella A, et al. Re-examining the role of TNF in MS pathogenesis and therapy. *Cell*. 2020;9:2290.

65. Robinson AP, Harp CT, Noronha A, et al. The experimental autoimmune encephalomyelitis (EAE) model of MS: utility for understanding disease pathophysiology and treatment. *Handb Clin Neurol*. 2014;122:173–189.

66. Taupitz M, Stolzenburg N, Ebert M, et al. Gadolinium-containing magnetic resonance contrast media: investigation on the possible transchelation of Gd^{3+} to the glycosaminoglycan heparin. *Contrast Media Mol Imaging*. 2013;8:108–116.

67. Popescu BF, Robinson CA, Rajput A, et al. Iron, copper, and zinc distribution of the cerebellum. *Cerebellum*. 2009;8:74–79.

68. White GW, Gibby WA, Tweedle MF. Comparison of Gd(DTPA-BMA) (Omniscan) versus Gd(HP-DO3A) (ProHance) relative to gadolinium retention in human bone

tissue by inductively coupled plasma mass spectroscopy. *Invest Radiol*. 2006;41:272–278.

69. Darrah TH, Prutsman-Pfeiffer JJ, Poreda RJ, et al. Incorporation of excess gadolinium into human bone from medical contrast agents. *Metallomics*. 2009;1:479–488.

70. Murata N, Murata K, Gonzalez-Cuyar LF, et al. Gadolinium tissue deposition in brain and bone. *Magn Reson Imaging*. 2016;34:1359–1365.

71. Ramalho J, Semelka RC, Ramalho M, et al. Gadolinium-based contrast agent accumulation and toxicity: an update. *AJNR Am J Neuroradiol*. 2016;37:1192–1198.

72. Thakral C, Abraham JL. Gadolinium-induced nephrogenic systemic fibrosis is associated with insoluble Gd deposits in tissues: in vivo transmetallation confirmed by microanalysis. *J Cutan Pathol*. 2009;36:1244–1254.

73. Gromov D, Toikka A. Toward formal analysis of thermodynamic stability: Le Chatelier-Brown principle. *Entropy (Basel)*. 2020;22:1113.

74. Bredholt M, Frederiksen JL. Zinc in multiple sclerosis: a systematic review and Meta-analysis. *ASN Neuro*. 2016;8:175909141665151.

75. Choi BY, Jung JW, Suh SW. The emerging role of zinc in the pathogenesis of multiple sclerosis. *Int J Mol Sci*. 2017;18:2070.

76. Puttagunta NR, Gibby WA, Smith GT. Human in vivo comparative study of zinc and copper transmetallation after administration of magnetic resonance imaging contrast agents. *Invest Radiol*. 1996;31:739–742.

77. Rasschaert M, Emerit A, Fretellier N, et al. Gadolinium retention, brain T1 Hyperintensity, and endogenous metals: a comparative study of macrocyclic versus linear gadolinium chelates in renally sensitized rats. *Invest Radiol*. 2018;53:328–337.

78. Humpel C. Organotypic brain slice cultures. *Curr Protoc Immunol*. 2018;123:e59.

79. Aktas O, Smorodchenko A, Brocke S, et al. Neuronal damage in autoimmune neuroinflammation mediated by the death ligand TRAIL. *Neuron*. 2005;46:421–432.

80. Tweedle MF, Wedeking P, Kumar K. Biodistribution of radiolabeled, formulated gadopentetate, gadoteridol, gadoterate, and gadodiamide in mice and rats. *Invest Radiol*. 1995;30:372–380.

81. Bower DV, Richter JK, von Tengg-Kobligk H, et al. Gadolinium-based MRI contrast agents induce mitochondrial toxicity and cell death in human neurons, and toxicity increases with reduced kinetic stability of the agent. *Invest Radiol*. 2019;54:453–463.

82. Xia Q, Feng X, Huang H, et al. Gadolinium-induced oxidative stress triggers endoplasmic reticulum stress in rat cortical neurons. *J Neurochem*. 2011;117:38–47.

83. Radbruch A, Richter H, Bücker P, et al. Is small fiber neuropathy induced by gadolinium-based contrast agents? *Invest Radiol*. 2020;55:473–480.

84. Smith AP, Marino M, Roberts J, et al. Clearance of gadolinium from the brain with no pathologic effect after repeated administration of gadodiamide in healthy rats: an analytical and histologic study. *Radiology*. 2017;282:743–751.

85. Habermeyer J, Boyken J, Harrer J, et al. Comprehensive phenotyping revealed transient startle response reduction and histopathological gadolinium localization to perineuronal nets after gadodiamide administration in rats. *Sci Rep*. 2020;10:22385.

86. Roccatagliata L, Vuolo L, Bonzano L, et al. Multiple sclerosis: hyperintense dentate nucleus on unenhanced T1-weighted MR images is associated with the secondary progressive subtype. *Radiology*. 2009;251:503–510.

87. Schlemm L, Chien C, Bellmann-Strobl J, et al. Gadopentetate but not gadobutrol accumulates in the dentate nucleus of multiple sclerosis patients. *Mult Scler*. 2017;23:963–972.

88. Forslin Y, Shams S, Hashim F, et al. Retention of gadolinium-based contrast agents in multiple sclerosis: retrospective analysis of an 18-year longitudinal study. *AJNR Am J Neuroradiol*. 2017;38:1311–1316.

89. Cocozza S, Pontillo G, Lanzillo R, et al. MRI features suggestive of gadolinium retention do not correlate with expanded disability status scale worsening in multiple sclerosis. *Neuroradiology*. 2019;61:155–162.

90. McDonald RJ, McDonald JS, Dai D, et al. Comparison of gadolinium concentrations within multiple rat organs after intravenous administration of linear versus macrocyclic gadolinium chelates. *Radiology*. 2017;285:536–545.